ACS OMEGA

Article

Cite This: ACS Omega 2018, 3, 2855−2864

Self-Assembly of Au@Ag Nanoparticles on Mussel Shell To Form Large-Scale 3D Supercrystals as Natural SERS Substrates for the Detection of Pathogenic Bacteria

Kaisong Yuan,[†,§,○] Junxia Zheng,[‡,○] Danting Yang,[∥] Beatriz Jurado Sánchez,[§,#] Xiangjiang Liu,[⊥] Xinjie Guo,[†] Chusheng Liu,[†] Nicoleta Elena Dina,[¶] Jingyi Jian,[†] Zhijun Bao,[†] Ziwei Hu,[†] Zhihong Liang,[▽] Haibo Zhou,*[,†] and Zhengjin Jiang*[,†]

[†]Institute of Pharmaceutical Analysis, College of Pharmacy, Jinan University, Guangzhou, Guangdong 510632, China

[‡]School of Chemical Engineering and Light Industry, Guangdong University of Technology, Guangzhou 510006, China

[§]Department of Analytical Chemistry, Physical Chemistry and Chemical Engineering, University of Alcala, Alcala de Henares E-28871, Madrid, Spain

[∥]Department of Preventative Medicine, Zhejiang Provincial Key Laboratory of Pathological and Physiological Technology, Medical School of Ningbo University, Ningbo, Zhejiang 315211, China

[⊥]College of Biosystems Engineering and Food Science, Zhejiang University, Hangzhou 310058, China

[#]Chemical Research Institute "Andrés M. del Río", University of Alcala, Alcala de Henares E-28871, Madrid, Spain

[¶]National Institute for Research and Development of Isotopic and Molecular Technologies, 67-103 Donat, 400293 Cluj-Napoca, Romania

[▽]Analysis and Test Center, Jinan University, Guangzhou, Guangdong 510632, China

Supporting Information

ABSTRACT: Herein, we developed a natural surface-enhanced Raman scattering (SERS) substrate based on size-tunable Au@Ag nanoparticle-coated mussel shell to form large-scale three-dimensional (3D) supercrystals (up to 10 cm^2) that exhibit surface-laminated structures and crossed nanoplates and nanochannels. The high content of $CaCO_3$ in the mussel shell results in superior hydrophobicity for analyte enrichment, and the crossed nanoplates and nanochannels provided rich SERS hot spots, which together lead to high sensitivity. Finite-difference time-domain simulations showed that nanoparticles in the channels exhibit apparently a higher electromagnetic field enhancement than nanoparticles on the platelets. Thus, under optimized conditions (using Au@AgNPs with 5 nm shell thickness), highly sensitive SERS detection with a detection limit as low as 10^{-9} M for rhodamine 6G was obtained. Moreover, the maximum electromagnetic field enhancement of different types of 3D supercrystals shows no apparent difference, and Au@AgNPs were uniformly distributed such that reproducible SERS measurements with a 6.5% variation (613 cm^{-1} peak) over 20 spectra were achieved. More importantly, the as-prepared SERS substrates can be utilized for the fast discrimination of *Escherichia coli*, *Staphylococcus aureus*, and *Pseudomonas aeruginosa* by discriminant analysis. This novel Au@Ag self-assembled mussel shell template holds considerable promise as low-cost, durable, sensitive, and reproducible substrates for future SERS-based biosensors.

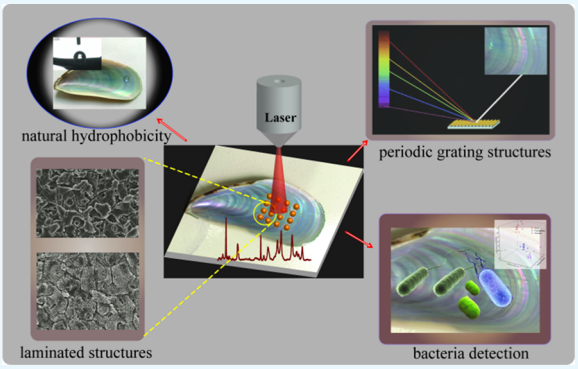

INTRODUCTION

The surface-enhanced Raman scattering (SERS) is a non-destructive and high ultrasensitive analytical technique that can provide "fingerprints" of molecules. It can be used as a qualitative tool in the analysis of unknown samples or to distinguish target molecules from a mixture of components. SERS relies on the enhancement of electromagnetic fields around metal nanoparticles to strongly increase Raman signals when molecules are attached to the nanoparticles.[1,2] In general, noble metals such as silver, gold, and copper are widely used as SERS active substrates with or without decoration.[3−5] Yet, the nanoprobes are used in solution, which results in random particle diffusion and heterogeneous distribution, ultimately leading to poor reproducibility in SERS detection.[6,7]

Received: January 4, 2018
Accepted: February 27, 2018
Published: March 9, 2018

DOI: 10.1021/acsomega.8b00023
ACS Omega 2018, 3, 2855−2864

A convenient way to improve SERS performance is to assemble metallic nanoparticles into three-dimensional (3D) structures. The hierarchical structure of such 3D structures results in the generation of ordered nanoparticles "clusters" with localized and abundant nanometer-level gaps to interact with the target molecules. In this way, more "hot spots" are created in a small area, and the SERS signals of absorbed analytes are enhanced.[8−11] For the creation of varying size, shape, and precise positioning of 3D nanostructures on support materials, many strategies such as electron beam lithography,[12,13] electrochemical deposition,[14,15] or magnetron sputtering[16,17] are normally employed. However, such methods are expensive, time-consuming, and require highly qualified personnel. Current trends are aimed to the use of natural 3D materials such as filter paper,[18] nanoporous zeolite[19] or silicon,[20] and cotton swab[21] as SERS templates. Yet, the low hydrophobicity of the above-mentioned materials prevents adequate analyte and nanoparticle enrichment for highly efficient SERS detection.

Recently, some natural materials with both 3D structures and hydrophobicity have been employed in the preparation of active SERS substrates. Because of its inherent hierarchical nanostructure, such materials can not only provide 3D structures to decorate nanoparticles, but also possess unique hydrophobicity to form beaded droplets on its surface. Droplet evaporation results in localized spots containing nanoparticles or analytes, and thus contributes to further increase in the SERS detection sensitivity.[22,23] For example, Huang et al. have demonstrated a highly efficient SERS substrate based on natural taro leaf decorated with silver nanoparticles (AgNPs). The micropapillae of the taro leaf exhibited hydrophobicity for analyte enrichment through the hydrophobic concentrating effect, and the secondary-crossed nanoplates acted as 3D templates to provide rich SERS hot spots after the decoration with AgNPs. Thereby, highly sensitive SERS detection with a detection limit as low as 10^{-8} M was achieved.[24] Sharma et al. employed five different types of plant leaf as the SERS substrate, in connection with gold nanoparticles (AuNPs). They found that the assembly helped by the hydrophobicity of plants surfaces helps to increase the SERS enhancement factor.[25] Rose petals have also been evaluated as 3D templates with natural hydrophobicity for the decoration of metal nanoparticles.[22,26] However, such materials lack periodic structures to ensure uniform distribution of the metal nanoparticles. As an alternative, cicada and butterfly wings with the hydrophobicity nature and ordered nanostructures were evaluated as SERS substrates.[27,28] Yet, their poor mechanical strength and short storage time hamper its practical application.

In this study, we aim to develop an SERS substrate through using the nacre from mussel shell as a new kind of natural material for the self-assembly of size-tunable Au@AgNPs. Natural mussel shells exhibit hydrophobicity because of its major inorganic composition of $CaCO_3$ and surface micro/nanohierarchical structures.[29] Thus, nanaoparticles (NPs) and analyte enrichment can be achieved to enhance the SERS sensitivity. The specific 3D hierarchical structures can be used as templates for the self-assembly of Au@Ag nanoparticles to form 3D supercrystals, which can lead to intense and controlled antenna effects, resulting in huge electromagnetic field.[30,31] Additionally, such laminated structures give the shell a twofold increase in strength and 1000-fold increase in roughness over its constituent materials.[32] Thus, the developed substrate will show obvious higher mechanical strength compared with other natural materials such as plant leaf, petals, cicada wings, and butterfly wings. More importantly, the grating microstructures of nacre on the mussel shell, which make the iridescence color of the shell because of the interference and diffraction of the natural light, are distributed periodically.[33] Such periodic grating microstructures will make the distribution of nanoparticles with high periodicity over the micrometer scale of the SERS substrate. Thus the signal reproducibility could be significantly improved at a large scale. Interestingly, some research works have shown that the interference and diffraction surface excitation caused by the periodic grating will benefit the SERS sensitivity.[34] Therefore, the nacre of mussel shell can act as a new kind of natural material in the preparation of SERS 3D supercrystals to display both higher sensitivity and signal reproducibility. Another aim is to employ the as-prepared Au@AgNPs self-assembled mussel shell substrate for the detection and discrimination of three different kinds of pathogenic bacteria.

RESULTS AND DISCUSSION

Optimization of the Metal Nanoparticles. Different kinds of metal nanoparticles and different shell thicknesses of Au@AgNPs may show different Raman enhancement activities after self-assembly on the mussel shell. To optimize the most suitable metal nanoparticles in the fabrication of mussel shell substrate, the SERS activity among different thicknesses of Au@AgNPs, AgNPs, and AuNPs has been evaluated.

First, transmission electron microscopy (TEM) has been used in the characterization of AgNPs and Au@AgNPs with different thicknesses of Ag shell. Figure 1a,b has shown the low-

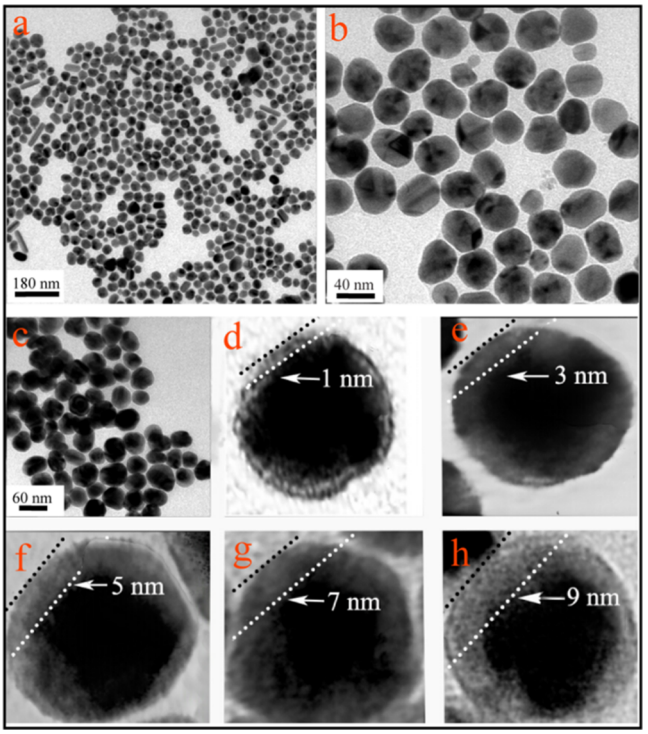

Figure 1. (a) Low-magnification TEM images of AgNPs. (b) High-magnification TEM of AgNPs. (c) Low-magnification TEM of Au@AgNPs with 5 nm thickness of Ag shell. (d−h) High-magnification TEM images of Au@AgNPs with Ag shell thicknesses of 1, 3, 5, 7, and 9 nm, respectively.

DOI: 10.1021/acsomega.8b00023
ACS Omega 2018, 3, 2855−2864

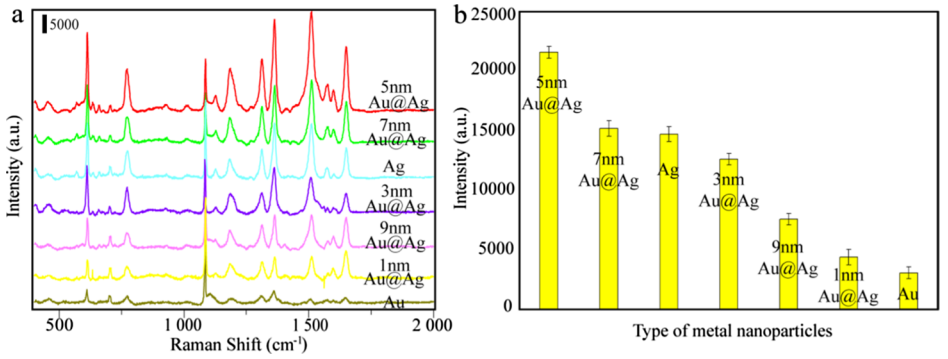

Figure 2. (a) SERS spectrum of mussel shell self-assembled with different kinds of metal nanoparticles. (b) Peaks intensity of SERS spectrum centered at 613 cm^{-1} corresponding to (a). The concentration of R6G was 10^{-3} M.

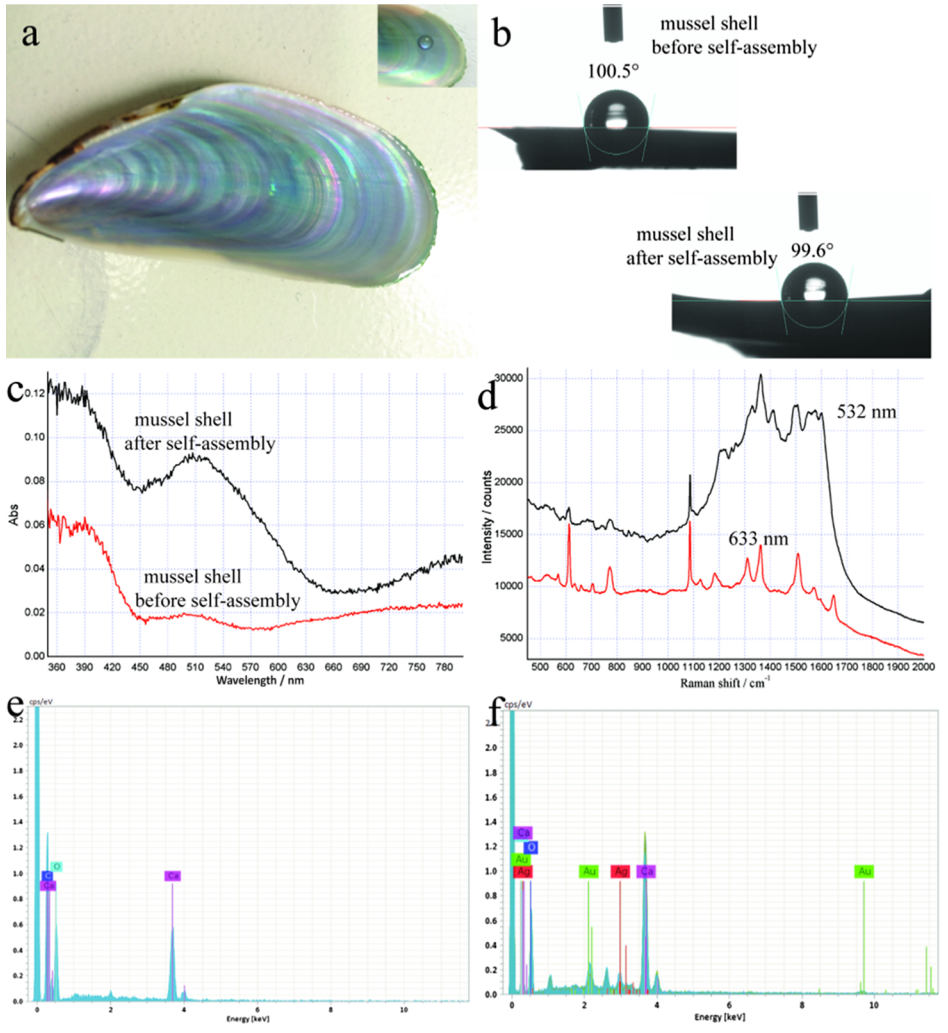

Figure 3. (a) Digital photograph of mussel shell, and the inset showing a water droplet on its surface. (b) CAs of mussel shell before and after the self-assembly of Au@AgNPs. (c) Optical absorption spectra of mussel shell before and after the self-assembly of Au@AgNPs. (d) SERS spectra of R6G solution recorded with two laser excitations. EDS spectra of mussel shell before (e) and after (f) the self-assembly of Au@AgNPs. Au@AgNPs with a 5 nm shell thickness were used in all cases.

magnification and high-magnification image of AgNPs. We can measure that the size of AgNPs is ~40 ± 12.5 nm. Figure 1c is the low magnification of Au@AgNPs with 5 nm thickness of Ag shell, which indicated that the sizes of the Au@AgNPs are uniform. Figure 1d–h (high magnification) showed that the thickness of Ag shells increased as the amount of $AgNO_3$ increased, and it can be seen that the Ag shells range from 1 to 9 nm for a fixed ~30 ± 5.6 nm Au core. It also can be clearly observed that Au@AgNPs become larger with the increase of the Ag shell thickness. The UV–vis absorbance spectra of the as-prepared Au@AgNPs with different Ag shell thicknesses also have been measured, and the results are shown in the Figure S2. It can be observed that as the thickness of the Ag shell increased, the absorption peak shifts from 510 to 400 nm.

DOI: 10.1021/acsomega.8b00023
ACS Omega 2018, 3, 2855–2864

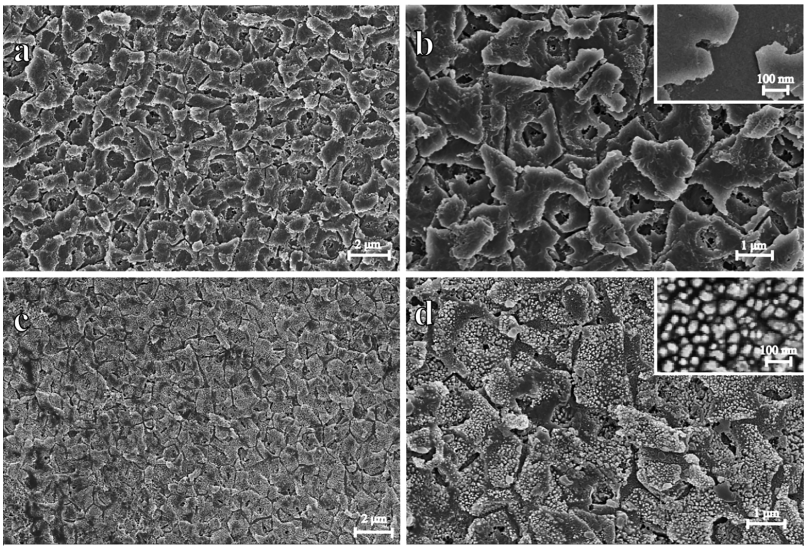

Figure 4. SEM of the blank and Au@AgNPs self-assembled mussel shell. (a,b) are both of the nanostructures of nacre on the shell before the self-assembly of Au@AgNPs. (c,d) are both of the nanostructures of nacre on the shell after the self-assembly of Au@AgNPs. The inset image on (b) is the higher magnification of the blank mussel shell, and the inset image on (d) show the higher magnification of Au@Ag self-assembled on the mussel shell substrate.

Subsequently, AuNPs, AgNPs, and Au@AgNPs with different Ag shell thicknesses have been self-assembled on the mussel shell under the same condition (20 μL of sample volume, room temperature) to evaluate their Raman enhancement activity. The concentrations of AuNPs used here is ∼0.26 nM, whereas AgNPs is ∼0.62 nM. The concentration of Au@AgNPs with different thicknesses of Ag shell is ∼0.18−0.25 nM. The stabilizer of both AuNPs (0.5 nM) and AgNPs (1.4 nM) is sodium citrate. The stabilizer of Au@AgNPs is ascorbic acid (10 mM). R6G (10^{-3} M) was used as the probe molecule. As depicted in Figure 2a,b, it is obvious that SERS intensity of bands is enhanced as the thickness of the Ag shell increases from 1 to 5 nm, and then decreased with Ag shell above 5 nm, which may because of the unstable and easily precipitate of the Au@AgNPs when the shell thicknesses are further increased.[35] Thus, we conclude that the SERS enhancement effect of Au@AgNPs is related to the Ag shell thickness. We also have compared the SERS activity of Au@AgNPs to AuNPs and AgNPs. Results showed that AuNPs show weakest SERS enhancement effect among these different kinds of nanoparticles, whereas AgNPs show SERS activity between 7 and 3 nm Au@AgNPs. Thus, the Au@AgNPs with a shell thickness of 5 nm have been used for the self-assembly of mussel shell in the following research.

Characterization of the Mussel Shell-Based Substrate. Figure 3a shows the photograph of a cleaned mussel shell. From the inset photograph, it is obvious that a water droplet can keep a sphere shape, which confirms its dewetting nature and indicates the hydrophobic property of it. As depicted in Figure 3b, the static water contact angle (CA) of the mussel shell was 100.5° before the self-assembly of nanoparticles, indicating the hydrophobic nature of the nacre mussel shell. Figure 3b also shows that the CA of the mussel shell is 99.6° after the self-assembly of Au@AgNPs with a shell thickness of 5 nm, indicating that the mussel shell still possesses hydrophobic property after the self-assembly of Au@AgNPs. Thus, these hydrophobic surfaces will accumulate the target molecule into a small size to enhance the SERS signals, even though the surfaces of the mussel shells are coated with nanoparticles.

Figure 3c shows the optical absorption spectra of Au@AgNPs (5 nm Ag shell thickness), self-assembled mussel shell, and the blank mussel shell. These two spectra all show adsorption peaks at 390 nm, attributed to the bare mussel shell. The spectra show the broad localized surface plasmon resonance (LSPR) absorption bands of Au@AgNPs at around 510 nm, which is different from its absorption spectrum in solution state (see Figure S2), indicating the formation of novel Au@AgNPs nanostructures onto the mussel shell. Previous studies have revealed that the LSPR is the major mechanism for SERS in the case of metal nanoparticles.[36] That is, the more wavelength match between surface plasmon band of the SERS substrate and the laser, the line may get higher SERS signals. Thus, the strongest SERS signals were obtained at 532 nm laser excitation. However, a large amount of fluorescence background signals existed in the SERS spectrum at 532 nm excitation, resulting in the loss of any useful information from Raman peaks (Figure 3d, red line). The better SERS performance was acquired with 633 nm excitation (Figure 3d, black line), which was then selected as optimal.

For the element analysis, energy-dispersive spectrometry (EDS) spectrum of elements indicates the presence of calcium, carbon, and oxygen on the mussel shell before the self-assembly of Au@AgNPs (Figure 3e). Such results are consistent with the previous reports which indicated that nacre shells are mainly composed by inorganic $CaCO_3$.[29] Figure 3f shows silver and gold distribution after the self-assembly of Au@AgNPs with a shell thickness of 5 nm, which reveals the presence of Au@AgNPs on the substrate.

The 3D structures of nacre on mussel shells were further characterized by scanning electron microscopy (SEM). Figure 4a,b shows low- and high-magnification images of the nanostructures of nacre on the shell before the self-assembly of Au@AgNPs. A clear distribution into polygon platelets can be clearly observed. This indicated that such natural material can provide specific 3D-laminated structures when used as templates for the self-assembly of Au@Ag nanoparticles. Importantly, such laminated structures give the shell a twofold increase in strength and a 1000-fold increase in toughness over

DOI: 10.1021/acsomega.8b00023
ACS Omega 2018, 3, 2855−2864

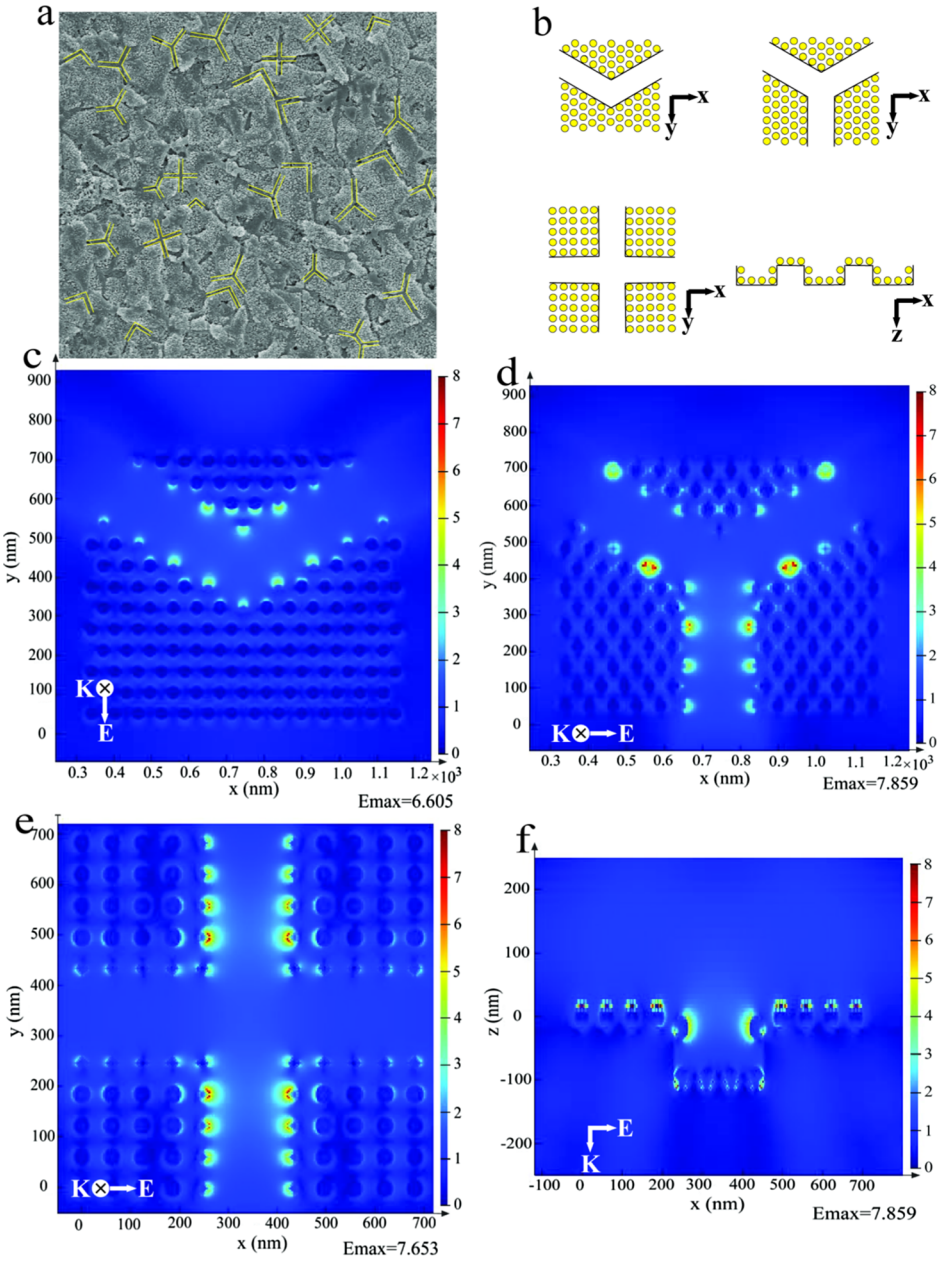

Figure 5. (a) SEM image of the mussel shell; (b) shape of the FDTD model of Au@AgNPs self-assembled mussel shell substrate; and (c−f) FDTD-simulated Ex-field enhancement of channels. The incident light with a wavelength of 633 nm enters in the z direction and is polarized in the x−y plane.

its constituent materials.[32] It should be mentioned here that the nacre shell substrate displays apparent higher mechanical strength compared with the other natural materials such as plant leaf, petals, or inset wings, acting thus as a more durable SERS substrate. For example, the mussel shell was hard to be damaged even after a pulling force experiment and kept its original state under the room temperature for a long time (Figure S3). Importantly, the Au@AgNPs self-assembled the mussel shell substrate can keep its high SERS activity for a long time (up to six months) and even at high temperature (Figure S4). Also, the toughness of the surface may contribute to the hydrophobicity of the shell. Figure 4c,d shows low- and high-magnification images of the nanostructure of the nacre on the shell after the self-assembly of Au@AgNPs. As can be seen, almost all of the polygon platelets of the mussel shell are fully coated with Au@AgNPs. These NPs were orderly arranged and homogeneously distributed along the laminated platelets of the mussel shell, the average gap between each adjacent NP which measured from 20 different random gaps is about 27 ± 5.9 nm. During the evaporation of the colloids, the spontaneous formation of the self-assembled supercrystals of Au@AgNPs takes place.[30,31] Thus, every laminated nanoplate was formed on 3D Au@AgNPs supercrystals, and the distribution of nanoplates results in different shapes of 3D supercrystals. The gap of two adjacent 3D supercrystals is about 220 ± 49.5 nm. Such features result in a large scale of 3D supercrystals arrays (up to 10 cm^2) (Figure S5). Therefore, the obtained novel 3D supercrystals will provide a robust substrate for application as SERS spot.

Additionally, the colorful nacre on the mussel shell contributed to the reproducibility of the as-prepared substrate to some extent. Figure S6a shows the nacre of the mussel shell

DOI: 10.1021/acsomega.8b00023
ACS Omega 2018, 3, 2855−2864

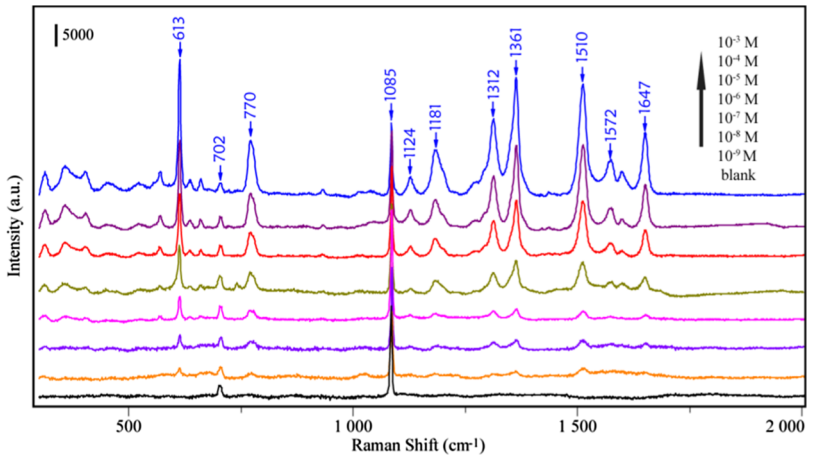

Figure 6. SERS spectra of R6G in the range of 1×10^{-3} to 1×10^{-9} M on the developed SERS substrate.

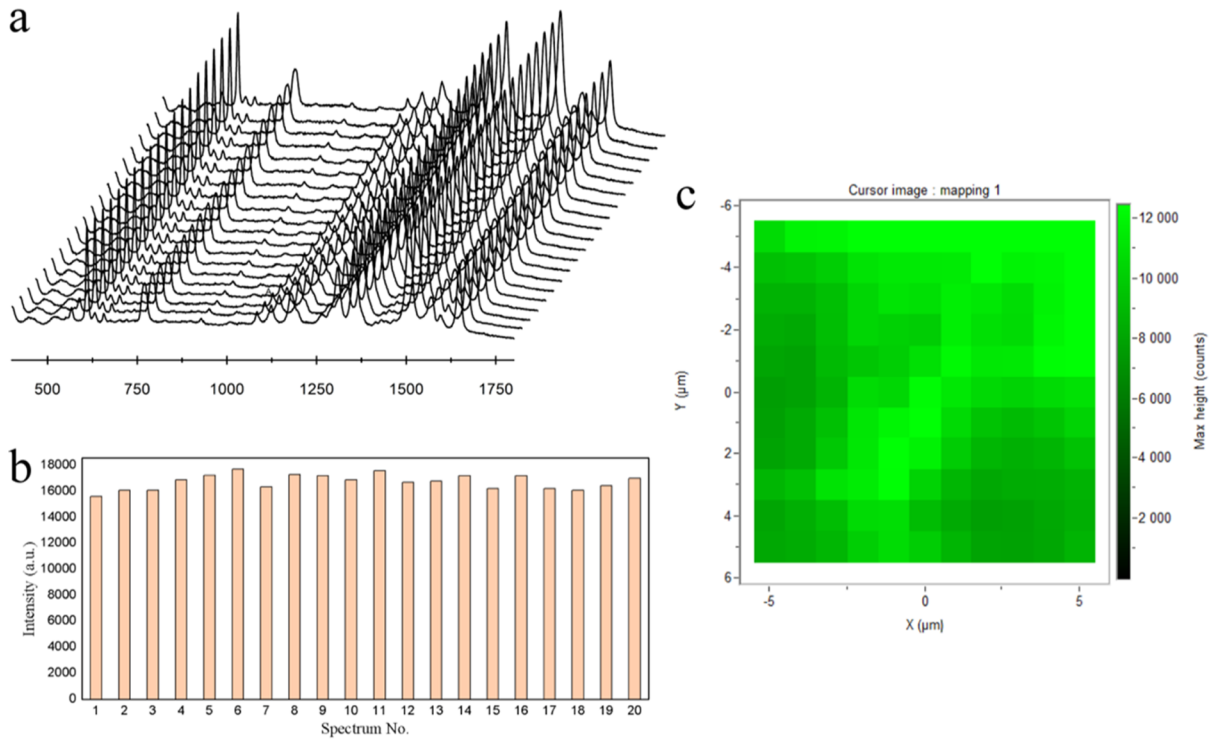

Figure 7. (a) SERS spectra of 5×10^{-4} M R6G collected from 20 random spots within an area of 100 μm^2. (b) Intensity distribution of the peaks centered at 613 cm^{-1} corresponding to (a) with the RSD of 6.5%. (c) SERS mapping (step size 1 μm, 10 μm × 10 μm = 100 μm^2) of one mussel shell substrate.

which was taken by a digital camera. We can see that its surface is colorful. Figure S6b shows the periodic grating microstructures of nacre on the mussel shell, which contribute to the iridescence color of the shell. Previous research works have proven that the groove density of the grating structure on the shell will exactly cause the diffraction of light.[37] The interference and diffraction surface excitation, caused by the periodic grating, will benefit SERS detection.[38] Thus, it is worth pointing out that the 3D hierarchical nanostructures, hydrophobicity, and periodic microstructures contribute to the high Raman enhancement and repeatability.

3D FDTD Simulation. We use the finite-difference time-domain (FDTD) method to study the spatial distribution of the electromagnetic fields according to the distribution of the Au@AgNPs acquired by SEM. As depicted in Figure 5a, the distribution of 3D supercrystals is in different modes (yellow lines), and it can be divided into three shapes of the FDTD model including "V" style, "Y" style, and "cross" style (Figure 5b). In this simulation, the diameter of Au@Ag nanoparticles was set at 35 nm, the width of the channel between two platelets was set as 220 nm, and the gap between two nanoparticles was set as 27 nm. The FDTD simulation based on such 3D supercrystals with different distribution modes of "V" style, "Y" style, and "cross" style is shown in Figure 5c–e. First of all, it can be obviously observed that nanoparticles in the channels (the edge of 3D supercrystals) exhibit apparent higher electromagnetic fields than nanoparticles on the platelets (inside the 3D supercrystals) in all of these distribution modes. This can theoretically prove that nanoparticles in channels between the polygon platelets will show higher SERS activity

DOI: 10.1021/acsomega.8b00023
ACS Omega 2018, 3, 2855−2864

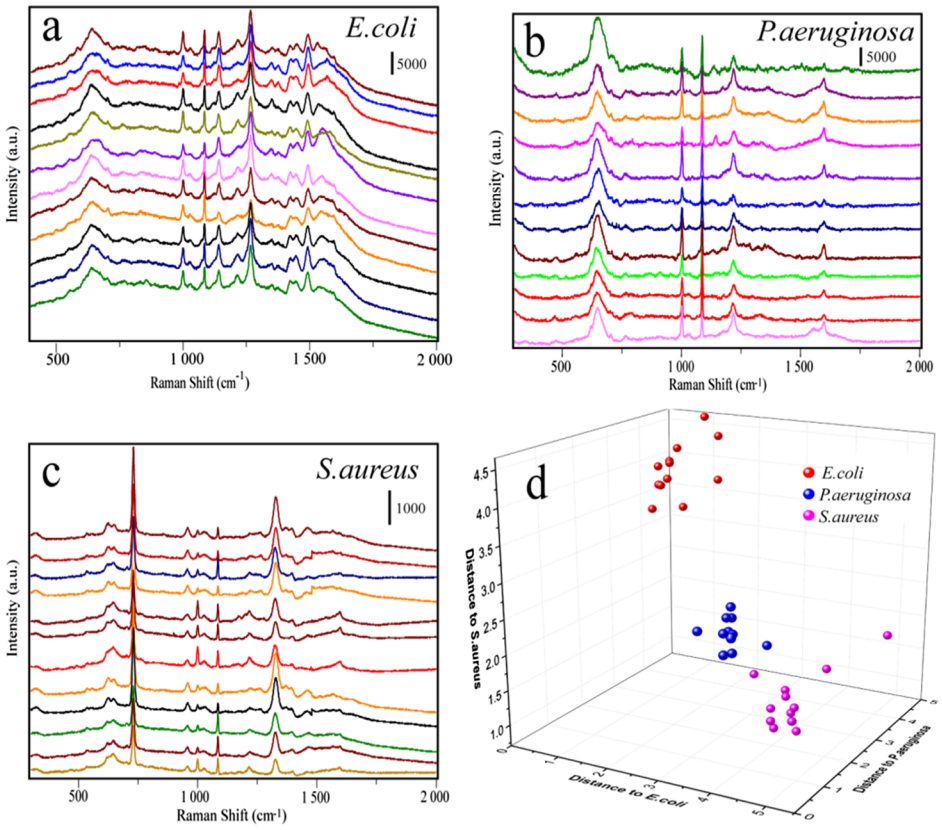

Figure 8. (a–c) SERS spectra of three different kinds of bacterium including *E. coli*, *P. aeruginosa*, and *S. aureus*. (d) DA plot showing discrimination among different kinds of bacterium.

than nanoparticles on the platelets. In other words, the mussel shell with natural platelets can serve as an excellent SERS substrate after the self-assembly of Au@AgNPs. Second, these three kinds of channels exhibit high electromagnetic field enhancement and show no apparent difference of the maximum electromagnetic field enhancement. This will make the distribution of electromagnetic field enhancement more uniform. Last, since different kinds of channel appear all over the whole mussel shell surface, the significantly enhanced electromagnetic field by the channels should dominate the enhancement of SERS signals, leading to high sensitivity and reproducibility. Figure 5f also showed the intersecting surface of these different kinds of channels on the mussel shell. We can observe that nanoparticles at the top of the channel show higher electromagnetic field enhancement than nanoparticles at the bottom of the channel, which is very useful to enhance the substrate absorption on the surface of 3D supercrystals. As the size of bacteria is larger than the channel, such target analytes thus cannot be absorbed into the channel.

SERS Performance. Figure 6 shows the SERS spectra of different concentrations of R6G droplets (20 μL) in the range of 1×10^{-3} to 1×10^{-9} M, which was detected after being evaporated naturally onto the 3D supercrystals. The Raman bands at 613, 770, and 1124 cm^{-1} can be assigned to C–C–C ring in-plane bending, C–H out-of-plane bending, and C–H in-plane bending, respectively. Other features at 1312, 1361, 1510, 1572, and 1647 cm^{-1} all stemmed from the aromatic C–C stretching vibrations. It can be seen that even at a concentration of 1×10^{-9} M, some peaks of R6G such as 613 and 770 cm^{-1} can be clearly identified. Additionally, the Raman bands at 702 and 1085 cm^{-1} come from the blank mussel shell. As described above, three aspects have contributed to such Raman enhancement. First of all, the hydrophobicity of the mussel shell helps to concentrate the Au@AgNPs and analytes into a small size. Second, the specific 3D structures of the mussel shell can act as a template for the self-assembly of Au@AgNPs to form 3D supercrystals. At last, the microstructures of the nacre on the mussel shell have a periodic grating, which will enhance the Raman signal to some extent. Thus, the 3D supercrystals' substrate will bring high and stable enhancement ability. An enhancement factor (EF) of 1.02×10^7 can be obtained (please see Figure S7 in the Supporting Information).

In addition to the high SERS enhancement ability, the as-prepared mussel shell-based substrate provided reproducible SERS signals. As depicted in Figure 7a, the SERS spectra of R6G from 20 random spots within an area of 100 μm^2 were recorded and the results showed that the SERS substrate provided uniform SERS enhancement upon its entire surface. Furthermore, we also compared the intensities of the 613 cm^{-1} peak of R6G, and the relative standard deviation (RSD) was calculated to be 6.5% (Figure 7b). To assess the spot-to-spot reproducibility, the mapping technique has been used by selecting 10 μm × 10 μm = 100 μm^2 area with a step size of 1 μm. As depicted in Figure 7c, the intensity of the 613 cm^{-1} peak from R6G was plotted to evaluate the uniformity of the entire SERS substrate, in which every pixel represents the intensity of the Raman peak at the spatial position on the mussel shell substrates. Results have shown that the as-prepared mussel shell substrate have a good uniformity and reproducibility over its entire area.

DOI: 10.1021/acsomega.8b00023
ACS Omega 2018, 3, 2855–2864

Table 1. Comparing SERS Performance of Different Kinds of Natural Materials

samples	ref	LOD (R6G) (M)	RSD	EF	durable of the original material	analytes
mussel shell	this work	10^{-9}	6.5%	10^{7}	high mechanical strength; keep original state for a long time	pathogenic bacteria
rose petal	22	10^{-15}	10.0%	10^{9}	weak mechanical strength withered in a short time	not available
taro leaf	24	10^{-8}	9.7%	10^{5}	weak mechanical strength withered in a short time	not available
cicada wing	27	10^{-7}	10.1%	10^{5}	weak mechanical strength keep original state for a long time	thiram
rose petal	26	10^{-9}	not available	10^{8}	weak mechanical strength withered in a short time	not available
butterfly wing	28	10^{-10}	9.0%	10^{6}	weak mechanical strength withered in a short time	tumor marker

Bacteria Detection. Sensitive and simultaneous detection of pathogenic bacteria is critical for human health because of many serious and fatal diseases caused by bacterial infections. In the label-free detection of bacteria, different kinds of bacteria will show special Raman fingerprints.[39] In this study, three kinds of bacteria including *Escherichia coli*, *Pseudomonas aeruginosa*, and *Staphylococcus aureus* have been chosen as models to investigate the potential of the mussel shell substrate in the discrimination of bacteria. The Raman spectra of *E. coli*, *P. aeruginosa*, and *S. aureus* from 36 batches (each kind of bacteria was represented by 12 batches) were acquired and depicted in Figure 8a–c. To maximize the spectral differences resulting from the data arrays in the discrimination of bacteria, discriminant analysis (DA) has been introduced here. Figure 8d shows the 3D map of the DA results, where red balls represent *E. coli*, green balls represent *P. aeruginosa*, and blue balls represent *S. aureus*. It can be seen that they are completely independent with each other in the space, which means that our SERS method combined with DA could be used to distinguish different kinds of bacteria.

CONCLUSIONS

In summary, we have developed a low-cost, durable, sensitive, and repeatable SERS substrate based on hydrophobic and nanohierarchical structures of mussel shell. Because of the hydrophobic concentration effect, Au@AgNPs and analyte molecules both aggregate on the mussel shell. The nanohierarchical structures could act as 3D templates for the self-assembly of nanoparticles to form 3D supercrystals. FDTD results have shown that nanoparticles in the channels exhibit apparent higher electromagnetic field enhancement than nanoparticles on the platelets. The distribution of nanoplates in different modes shows no apparent difference of the maximum electromagnetic field enhancement, which makes the distribution of electromagnetic field enhancement more uniform. The periodic gratings on the mussel shell also have made the distribution of nanoparticles with high periodicity on the SERS substrate. All of these have revealed that the special structure of the nacre makes the mussel shell a good candidate for the decoration of nanoparticles to form 3D supercrystals. As a result, the 3D supercrystals could reach an LOD (limit of detection) for R6G as low as 1×10^{-9} M, and signal reproducibility could be significantly improved and measured with a variation of 6.5% at the peak of 613 cm^{-1}. The as-prepared SERS substrate also has been utilized in the discrimination of different kinds of pathogenic bacteria. As shown in Table 1, the mussel shell has demonstrated obvious advantages compared to other natural materials, and it can act as a good substrate for the detection of other practical analytes.

EXPERIMENTAL SECTION

Chemicals, Biochemicals, and Instruments. Mussel shells were purchased from the local market in China. Rhodamine 6G (Rh6G), chloroauric acid tetrahydrate ($HAuCl_4 \cdot 4H_2O$), trisodium citrate, and ascorbic acid were supplied by Macklin (Shanghai, China). Silver nitrate ($AgNO_3$) was purchased from Aladdin. Ultrapure water was obtained using a Millipore water purification system. All chemicals were of the analytical grade. *E. coli* (ATCC8739), *S. aureus* (ATCC6538), and *P. aeruginosa* (PAO1) shock-frozen strains were purchased from Guangdong Microbial Culture Center (Guangdong, China).

The morphologies and microstructures of the mussel shell-based substrate were investigated by field-emission scanning electron microscopy (ZEISS ULTRA55), and the core–shell structures Au@AgNPs were characterized using a transmission electron microscope (JEM-2100F). UV–vis spectra were recorded with a Varian Cary-5000 UV–vis–NIR spectrophotometer. SERS measurements were conducted with a Raman microscope (LabRAM HR, HORIBA Scientific, Japan). The CA was measured with OCA20 machine (Data Physics, Germany).

Preparation of Au and Ag Nanoparticles (AuNPs). Before use, all glassware were soaked in 3:1 HNO_3/HCl overnight, followed by ultrapure water and dried in the dry oven. AuNPs and AgNPs were all prepared according to the previous report with some modifications.[40] First, 125 μL of $HAuCl_4$ solution (0.1 M) was added to 50 mL of boiling ultrapure water under magnetic stirring. Subsequently, 750 μL of trisodium citrate (1%) was added, and the solution was agitated for 30 min to obtain a wine-red suspension. After the suspension was cooled to room temperature, the as-prepared AuNPs were filtered through a 0.22 μm Millipore membrane and stored at 4 °C. For Ag nanoparticle preparation, 90 mg of $AgNO_3$ was first dissolved in 250 mL of ultrapure water and brought to boiling. Then, 10 mL trisodium citrate (1%) was added into the above solution and kept boiling for 1 h. The AgNP colloids were obtained after cooling to room temperature. The calculation of concentrations of AuNPs and AgNPs is based on the Beer's law and the extinction coefficient ($\varepsilon_{Au} = 3 \times 10^9$ M^{-1} cm^{-1} and $\varepsilon_{Ag} = 2.3 \times 10^{10}$ M^{-1} cm^{-1}). Thus, the concentrations of AuNPs and AgNPs are ~0.26 and ~0.62 nM.[35]

Synthesis of Au@Ag Nanoparticles with Different Ag Shell Thickness. All glassware were treated with 3:1 HNO_3/HCl and ultrasonically with deionized water prior to use. Au@AgNPs were prepared through the reduction of silver nitrate onto the surface of as-prepared AuNPs, according to the previous report.[41] In a 50 mL flask, 10 mL of the as-prepared AuNPs and 1.5 mL of ascorbic acid (0.1 M) were mixed and kept under stirring. Then, 1 mM $AgNO_3$ was added drop by drop and stirred for 30 min at room temperature. For different thicknesses of Ag shells from 1 to 9 nm, the volumes of 1 mM $AgNO_3$ solution were increased from 0.5 to 4.5 mL. The as-prepared Au@AgNPs with different Ag shell thicknesses were stored at 4 °C for the further self-assembly with mussel shell.

DOI: 10.1021/acsomega.8b00023
ACS Omega 2018, 3, 2855–2864

The final concentration of Au@AgNPs is ∼0.18−0.25 nM, as calculated based on Au cores and the change of volume.[35]

Fabrication of SERS Substrates. The mussels obtained commercially were first scalded with boiling water for a moment, and the meats were removed from the shell. Then, the mussel shells were washed in an ultrasound bath with ethanol and deionized water in turn for 10 min individually. As depicted in Figure S1, a 20 μL droplet of a suspension of different Ag shell thickness of Au@AgNPs was placed on the nacre of the mussel shell and allowed to dry naturally. For different experimental aims, a 20 μL droplet of rhodamine 6G with different concentrations were then placed on the SERS substrate and allowed to dry again.

Bacteria Preparation and SERS Measurements. Shock-frozen *E. coli*, *P. aeruginosa*, and *S. aureus* cells were cultivated in Luria−Bertani medium in a gyratory shaker at 100 rpm and 37 °C for 16 h. Five milliliters of bacteria were harvested and washed twice with deionized water by centrifugation at 4000 rpm and 25 °C. Subsequently, the obtained bacteria were utilized for the SERS measurement.

The Raman signals of R6G and three different kinds of bacteria were obtained after the droplet evaporated naturally and measured on the Raman system with the 633 nm laser as excitation. The power density of the laser is 16.0 mW/μm^2. A 50× objective lens was used, and the time acquisition was 5 s.

■ ASSOCIATED CONTENT

Supporting Information

The Supporting Information is available free of charge on the ACS Publications website at DOI: 10.1021/acsomega.8b00023.

Process flow of concentrating Au@AgNPs and analytes on the nacre of mussel shell; UV−vis spectra of Au@AgNPs with different Ag shell thickness; mechanical properties among mussel shell and other different kinds of natural materials; stability of Au@AgNPs self-assembled mussel shell SERS substrate; large scale of the mussel shell substrate; colorful nacre on the mussell shell and SEM image of the periodic grating microstructures of nacre; and Raman spectrum of R6G powder and SERS spectra of R6G solution (PDF)

■ AUTHOR INFORMATION

Corresponding Authors

*E-mail: haibo.zhou@jnu.edu.cn (H.Z.).
*E-mail: jzjjackson@hotmail.com (Z.J.).

ORCID

Beatriz Jurado Sánchez: 0000-0002-6584-1949
Xiangjiang Liu: 0000-0002-5419-669X
Nicoleta Elena Dina: 0000-0002-0435-2105
Haibo Zhou: 0000-0002-0098-5968

Author Contributions

°K.Y. and J.Z. contributed equally.

Notes

The authors declare no competing financial interest.

■ ACKNOWLEDGMENTS

This work was supported by the National Natural Science Foundation of China (nos. 21505053, 81773684, 21405138, and 81773593), the Pearl River S&T Nova Program of Guangzhou (201806010060 and 201610010100), the Science and Technology Planning Project of Guangdong Province, China (nos. 2015A020211018, 2015A030401045, and 2016A030310089), the Excellent Young Teachers Program of Guangdong Provincial colleges and universities (YQ 2015061), the Science Foundation of Zhejiang Province (no. LY17H260003), and the Ningbo Natural Science Foundation (no. 2017A610226).

■ REFERENCES

(1) Ding, S.-Y.; You, E.-M.; Tian, Z.-Q.; Moskovits, M. Electromagnetic theories of surface-enhanced Raman spectroscopy. *Chem. Soc. Rev.* **2017**, *46*, 4042−4076.
(2) Tang, L.; Li, S.; Han, F.; Liu, L.; Xu, L.; Ma, W.; Kuang, H.; Li, A.; Wang, L.; Xu, C. SERS-active Au@Ag nanorod dimers for ultrasensitive dopamine detection. *Biosens. Bioelectron.* **2015**, *71*, 7−12.
(3) Zhou, H.; Yang, D.; Ivleva, N. P.; Mircescu, N. E.; Niessner, R.; Haisch, C. SERS detection of bacteria in water by in situ coating with Ag nanoparticles. *Anal. Chem.* **2014**, *86*, 1525−1533.
(4) Mei, Q.; Jing, H.; Li, Y.; Yisibashaer, W.; Chen, J.; Li, B. N.; Zhang, Y. Smartphone based visual and quantitative assays on upconversional paper sensor. *Biosens. Bioelectron.* **2016**, *75*, 427−432.
(5) Chen, K.; Zhang, X.; MacFarlane, D. R. Ultrasensitive surface-enhanced Raman scattering detection of urea by highly ordered Au/Cu hybrid nanostructure arrays. *Chem. Commun.* **2017**, *53*, 7949−7952.
(6) Wu, Y.; Hang, T.; Komadina, J.; Ling, H.; Li, M. High-adhesive superhydrophobic 3D nanostructured silver films applied as sensitive, long-lived, reproducible and recyclable SERS substrates. *Nanoscale* **2014**, *6*, 9720−9726.
(7) Hasna, K.; Antony, A.; Puigdollers, J.; Kumar, K. R.; Jayaraj, M. K. Fabrication of cost-effective, highly reproducible large area arrays of nanotriangular pillars for surface enhanced Raman scattering substrates. *Nano Res.* **2016**, *9*, 3075−3083.
(8) Chen, B.; Meng, G.; Huang, Q.; Huang, Z.; Xu, Q.; Zhu, C.; Qian, Y.; Ding, Y. Green synthesis of large-scale highly ordered core@shell nanoporous Au@Ag nanorod arrays as sensitive and reproducible 3D SERS substrates. *ACS Appl. Mater. Interfaces* **2014**, *6*, 15667−15675.
(9) Zhang, Q.; Lee, Y. H.; Phang, I. Y.; Lee, C. K.; Ling, X. Y. Hierarchical 3D SERS substrates fabricated by integrating photolithographic microstructures and self-assembly of silver nanoparticles. *Small* **2014**, *10*, 2703−2711.
(10) Zhang, X.; Xiao, X.; Dai, Z.; Wu, W.; Zhang, X.; Fu, L.; Jiang, C. Ultrasensitive SERS performance in 3D "sunflowerlike" nanoarrays decorated with Ag nanoparticles. *Nanoscale* **2017**, *9*, 3114.
(11) Liu, H.; Yang, L.; Liu, J. Three-dimensional SERS hot spots for chemical sensing: Towards developing a practical analyzer. *TrAC, Trends Anal. Chem.* **2016**, *80*, 364−372.
(12) Chirumamilla, M.; Chirumamilla, A.; Roberts, A. S.; Zaccaria, R. P.; De Angelis, F.; Kristensen, P. K.; Krahne, R.; Bozhevolnyi, S. I.; Pedersen, K.; Toma, A. Hot-spot engineering in 3D multi-branched nanostructures: Ultrasensitive substrates for surface-enhanced Raman spectroscopy. *Adv. Opt. Mater.* **2017**, *5*, 1600836.
(13) Hatab, N. A. A.; Oran, J. M.; Sepaniak, M. J. Surface-enhanced Raman spectroscopy substrates created via electron beam lithography and nanotransfer printing. *ACS Nano* **2008**, *2*, 377−385.
(14) Yang, S.; Lapsley, M. I.; Cao, B.; Zhao, C.; Zhao, Y.; Hao, Q.; Kiraly, B.; Scott, J.; Li, W.; Wang, L.; Lei, Y.; Huang, T.J. Large-Scale fabrication of three-dimensional surface patterns using template-defined electrochemical deposition. *Adv. Funct. Mater.* **2013**, *23*, 720−730.
(15) Yang, S.; Slotcavage, D.; Mai, J. D.; Guo, F.; Li, S.; Zhao, Y.; Lei, Y.; Cameron, C. E.; Huang, T. J. Electrochemically created highly surface roughened Ag nanoplate arrays for SERS biosensing applications. *J. Mater. Chem. C* **2014**, *2*, 8350−8356.
(16) Zhang, J.; Zhang, X.; Chen, S.; Gong, T.; Zhu, Y. Surface-enhanced Raman scattering properties of multi-walled carbon nanotubes arrays-Ag nanoparticles. *Carbon* **2016**, *100*, 395−407.

DOI: 10.1021/acsomega.8b00023
ACS Omega 2018, 3, 2855−2864

(17) Cui, S.; Dai, Z.; Tian, Q.; Liu, J.; Xiao, X.; Jiang, C.; Wu, W.; Roy, V. A. L. Wetting properties and SERS applications of ZnO/Ag nanowire arrays patterned by a screen printing method. *J. Mater. Chem. C* **2016**, *4*, 6371−6379.
(18) Lee, C. H.; Hankus, M. E.; Tian, L.; Pellegrino, P. M.; Singamaneni, S. Highly sensitive surface enhanced Raman scattering substrates based on filter paper loaded with plasmonic nanostructures. *Anal. Chem.* **2011**, *83*, 8953−8958.
(19) Liu, N.; Gong, M.; Zhang, P.; Li, L.; Li, W.; Lee, R. Silver-embedded zeolite crystals as substrates for surface-enhanced Raman scattering. *J. Mater. Sci.* **2011**, *46*, 3162−3168.
(20) Novara, C.; Marta, S. D.; Virga, A.; Lamberti, A.; Angelini, A.; Chiadò, A.; Rivolo, P.; Geobaldo, F.; Sergo, V.; Bonifacio, A.; Giorgis, F. SERS-active Ag nanoparticles on porous silicon and PDMS substrates: A comparative study of uniformity and Raman efficiency. *J. Phys. Chem. C* **2016**, *120*, 16946−16953.
(21) Gong, Z.; Du, H.; Cheng, F.; Wang, C.; Wang, C.; Fan, M. Fabrication of SERS swab for direct detection of trace explosives in fingerprints. *ACS Appl. Mater. Interfaces* **2014**, *6*, 21931−21937.
(22) Chou, S.-Y.; Yu, C.-C.; Yen, Y.-T.; Lin, K.-T.; Chen, H.-L.; Su, W.-F. Romantic story or Raman scattering? Rose petals as ecofriendly, low-cost substrates for ultrasensitive surface-enhanced Raman scattering. *Anal. Chem.* **2015**, *87*, 6017−6024.
(23) Koch, K.; Bhushan, B.; Barthlott, W. Diversity of structure, morphology and wetting of plant surfaces. *Soft Matter* **2008**, *4*, 1943−1963.
(24) Huang, J.-A.; Zhang, Y.-L.; Zhao, Y.-Q.; Zhang, X.-L.; Sun, M.-L.; Zhang, W. Superhydrophobic SERS chip based on Ag coated natural taro-leaf. *Nanoscale* **2016**, *8*, 11487−11493.
(25) Sharma, V.; Kumar, S.; Jaiswal, A.; Krishnan, V. Gold deposited plant leaves for SERS: Role of surface morphology, wettability and deposition technique in determining the enhancement factor and sensitivity of detection. *ChemistrySelect* **2017**, *2*, 165−174.
(26) Xu, B.-B.; Zhang, Y.-L.; Zhang, W.-Y.; Liu, X.-Q.; Wang, J.-N.; Zhang, X.-L.; Zhang, D.-D.; Jiang, H.-B.; Zhang, R.; Sun, H.-B. Silver-coated rose petal: Green, facile, low-cost and sustainable fabrication of a SERS substrate with unique superhydrophobicity and high efficiency. *Adv. Opt. Mater.* **2013**, *1*, 56−60.
(27) Lv, M. Y.; Teng, H. Y.; Chen, Z. Y.; Zhao, Y. M.; Zhang, X.; Liu, L.; Wu, Z.; Liu, L. M.; Xu, H. J. Low-cost Au nanoparticle-decorated cicada wing as sensitive and recyclable substrates for surface enhanced Raman scattering. *Sens. Actuators, B* **2015**, *209*, 820−827.
(28) Song, G.; Zhou, H.; Gu, J.; Liu, Q.; Zhang, W.; Su, H.; Su, Y.; Yao, Q.; Zhang, D. Tumor marker detection using surface enhanced Raman spectroscopy on 3D Au butterfly wings. *J. Mater. Chem. B* **2017**, *5*, 1594.
(29) Liu, X.; Zhou, J.; Xue, Z.; Gao, J.; Meng, J.; Wang, S.; Jiang, L. Clam's shell inspired high-energy inorganic coatings with underwater low adhesive superoleophobicity. *Adv. Mater.* **2012**, *24*, 3401−3405.
(30) Alvarez-Puebla, R. A.; Agarwal, A.; Manna, P.; Khanal, B. P.; Aldeanueva-Potel, P.; Carbo-Argibay, E.; Pazos-Perez, N.; Vigderman, L.; Zubarev, E. R.; Kotov, N. A.; Liz-Marzan, L. M. Gold nanorods 3D-supercrystals as surface enhanced Raman scattering spectroscopy substrates for the rapid detection of scrambled prions. *Proc. Natl. Acad. Sci. U. S. A.* **2011**, *108*, 8157−8161.
(31) Gómez-Graña, S.; Pérez-Juste, J.; Alvarez-Puebla, R. A.; Guerrero-Martínez, A.; Liz-Marzán, L. M. Self-Assembly of Au@Ag nanorods mediated by gemini surfactants for highly efficient SERS-active supercrystals. *Adv. Opt. Mater.* **2013**, *1*, 477−481.
(32) Li, X.; Chang, W.-C.; Chao, Y. J.; Wang, R.; Chang, M. Nanoscale structural and mechanical characterization of a natural nanocomposite material: The shell of red abalone. *Nano Lett.* **2004**, *4*, 613−617.
(33) Snow, M. R.; Pring, A.; Self, P.; Losic, D.; Shapter, J. The origin of the color of pearls in iridescence from nano-composite structures of the nacre. *Am. Mineral.* **2004**, *89*, 1353−1358.
(34) Shen, Y.; Cheng, X.; Li, G.; Zhu, Q.; Chi, Z.; Wang, J.; Jin, C. Highly sensitive and uniform surface-enhanced Raman spectroscopy from grating-integrated plasmonic nanograss. *Nanoscale Horiz.* **2016**, *1*, 290−297.
(35) Liu, B.; Han, G.; Zhang, Z.; Liu, R.; Jiang, C.; Wang, S.; Han, M.-Y. Shell thickness-dependent Raman enhancement for rapid identification and detection of pesticide residues at fruit peels. *Anal. Chem.* **2011**, *84*, 255−261.
(36) Tanahashi, I.; Harada, Y. Silver nanoparticles deposited on TiO_2-coated cicada and butterfly wings as naturally inspired SERS substrates. *J. Mater. Chem. C* **2015**, *3*, 5721.
(37) Liu, Y.; Shigley, J.; Hurwit, K. Iridescence color of a shell of the mollusk Pinctada Margaritifera caused by diffraction. *Opt. Express* **1999**, *4*, 177−182.
(38) Xu, S.; Xu, W.; Li, H. Method for detecting surface enhanced Raman spectrum based on interference and diffraction stimulation. E.U. Patent CN201010524200, 2010.
(39) Zhou, H.; Yang, D.; Ivleva, N. P.; Mircescu, N. E.; Schubert, S.; Niessner, R.; Wieser, A.; Haisch, C. Label-free in situ discrimination of live and dead bacteria by surface-enhanced Raman scattering. *Anal. Chem.* **2015**, *87*, 6553−6561.
(40) Hu, Z.; Xie, M.; Yang, D.; Chen, D.; Jian, J.; Li, H.; Yuan, K.; Jiang, Z.; Zhou, H. A simple, fast, and sensitive colorimetric assay for visual detection of berberine in human plasma by $NaHSO_4$-optimized gold nanoparticles. *RSC Adv.* **2017**, *7*, 34746−34754.
(41) Olson, T. Y.; Schwartzberg, A. M.; Orme, C. A.; Talley, C. E.; O'Connell, B.; Zhang, J. Z. Hollow gold-silver double-shell nanospheres: structure, optical absorption, and surface-enhanced Raman scattering. *J. Phys. Chem. C* **2008**, *112*, 6319−6329.

DOI: 10.1021/acsomega.8b00023
ACS Omega 2018, 3, 2855−2864